12-2006

A Simple Numerical Method of Cycle Jumps for Cyclically Loaded Structures

D. Cojocaru
University of Delaware

Anette M. Karlsson
Cleveland State University, a.karlsson@csuohio.edu

Publisher's Statement

NOTICE: this is the author's version of a work that was accepted for publication in International Journal of Fatigue. Changes resulting from the publishing process, such as peer review, editing, corrections, structural formatting, and other quality control mechanisms may not be reflected in this document. Changes may have been made to this work since it was submitted for publication. A definitive version was subsequently published in International Journal of Fatigue, 28, 12, (12-01-2006); 10.1016/j.ijfatigue.2006.01.010

Original Citation

Cojocaru, D., and Karlsson, A. M., 2006, "A Simple Numerical Method of Cycle Jumps for Cyclically Loaded Structures," International Journal of Fatigue, 28(12) pp. 1677-1689.

A simple numerical method of cycle jumps for cyclically loaded structures

D. Cojocaru, A.M. Karlsson *

Department of Mechanical Engineering, University of Delaware, 126 Spencer Laboratory, Newark, DE 19716, United States

1. Introduction

Failures of structures subjected to cyclic loading are often influenced by a slow evolution of material properties. For example, over the lifetime of the structure, yield-strength or elastic modulus may change and eigen-strains may develop due to phase transformation. Factors such as thermal exposure (e.g. thermal barrier coatings [1–3]), humidity (e.g. fuel cells [4], silica glass [5]), and environmental attacks (e.g. corrosion [6–8], irradiation [9]) can cause a change in material properties. Design against failure for this class of structures is associated with many challenges, including determining the material properties as they evolve with time and how the stress state of the structure change within each load cycle and with long term exposure. Finite element analysis (FEA) is a convenient tool that readily gives a stress and strain distribution as a function of time when individual load cycles are simulated, and where material properties from experimental results can easily be incorporated, e.g., [10–12]. However, due to the intrinsic non-linearities associated with complex systems – such as non-linear, temperature dependent material properties – a single load cycle in FEA normally consist of many numerical increments and iterations. Thus, simulating each cycle a structure goes through before fatigue failure occurs is many times not feasible.

In this paper, we will focus on modeling aspects of structures with evolving properties subjected to cyclic loading. In particular, we will investigate a method of accelerated FEA, where not all individual cycles need to be modeled. We aim to develop a numerical technique that shortens the simulations, by utilizing the general concept of "cycle-jump". This will eliminate the need of simulating each individual cycle and significantly reduce the need for extensive experimental investigations. The method assumes knowledge of the evolving properties. However, if these properties are not known, the model can instead be used for reverse analysis, i.e., determining properties from experimental observations.

Here, a class of structures with slowly evolving structural properties will be considered. An example of structure with such features relates to thermal barrier coatings discussed below. However, the model is not limited to thermal

* Corresponding author. Tel.: +1 302 831 6437.
E-mail address: karlsson@me.udel.edu (A.M. Karlsson).

barrier coatings but can be used for any structure with evolving material properties or slowly changing boundary conditions.

The concept of cycle jumps has been investigated by several authors. The "Large Time Increments Method" (LATIN Method) was introduced in the early 1990's by Ladevèze and co-workers [13,14]. This method separates the equations of the initial boundary value problem into two groups: (i) linear equations, global in space; and (ii) non-linear equations, which are local in space. Even though the theory behind the "LATIN method" is interesting, the implementation into commercial FEA software tends to be too cumbersome in its current form to be of practical interest. Fish and coworkers [15,16] have developed an alternative method for cycle jumps where the time is decomposed into two time scales: one micro-chronological (fast time scale) and one macro-chronological (slow time scale). Thus, the micro-chronological time corresponds to the cyclic behavior, and the macro-chronological to the overall trend of the structure. Even though the concept is sound, there are some challenges with implementing the method into commercial finite element programs. Kiewel et al. [17] developed a method to extrapolate the complete set of internal variables over a certain range of cycles. The extrapolation is based on piecewise polynomial or spline functions that are formed for each integration point in the finite element model. As for the previous models mentioned, the method is customized for viscoplastic material. A simple cycle-jump scheme was proposed in [18] by Van Paepegem et al. based on extrapolation of the damage parameter by using the explicit Euler integration formula. This method performs automatic computations of the jump length. A local computation (at each integration point) is accomplished by imposing a user supplied maximum allowed increment/jump for the damage variable. The global jump length is then obtained as the abscisae value for which the cumulative statistical distribution of locally determined jump length reached a certain percent (10%) which is empirically provided by the user.

All of the above methods are based on some variant of damage theory, whereas our method is based on *evolving properties*. This could include damage theory but in this feasibility study, we study the effect of transformation strains, discussed below. The proposed method allows for both time and/or temperature dependent structural changes such as increasing elastic modulus due to high-temperature sintering; geometry changes due to oxidation, or permanent non-linear deformation; changing yield strength due to high temperature diffusion or eigen-strain due to phase transformations. Needless to say, the cyclic nature of this set of problems results in a completely different state than if the structure was subjected to a static load [10,19].

The typical evolution with time of either a primary or a secondary dependent variable (such as a displacement, strain or stress component) is shown in Fig. 1. As the structure is cyclically loaded (where "load" can be force, displacement, temperature or any other external parameter

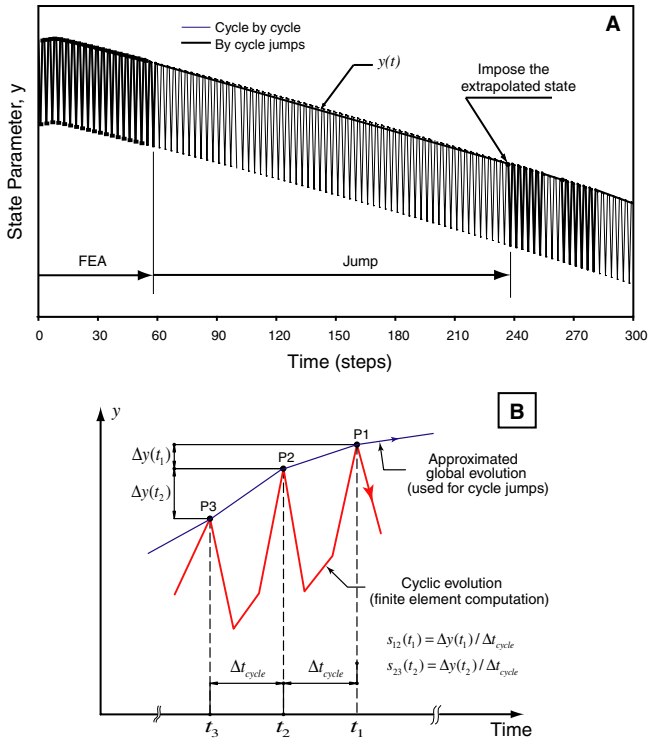

Fig. 1. A schematic of an evolving state parameter, $y(t)$, for a structure subjected to cyclic loading.

that will affect the state variables), the state variables will change slightly after each full cycle, Fig. 1. Thus, a local and a global change in the variable occur, where the local is the high frequency variation and the global corresponding to the general, long term trend. If the general trend can be expressed as a mathematical function, this function can be used to extrapolate the state variable. We will refer to this function as the "global evolution function." Thus, utilizing the global evolution function, the long-term response of the structure can be determined, or at least approximated, without having to model the details of all cycles.

The overall goal of this work is to develop a method that can reduce the computational effort by performing cycle jumps along the global evolution of structural properties. To achieve this, our general approach is:

1. Conduct a set of cycles in FEA to establish the trend line, i.e., the global evolution function for each structural variable;
2. Extrapolate the state using the global evolution functions;
3. Impose the extrapolated state as the initial state for a new finite element analysis after the cycle jump.

A major challenge is to judge the success of the cycle jump. We will see later that convergence of the FEA is not guarantee for a correct solution. Therefore, an extrapolation scheme including a "control function" is needed to enhance the accuracy of the calculation, controlling the length of the cycle jumps. This will be explored in the following.

2. Concept and modeling of cycle jumps

The system that has inspired us in this investigation, thermal barrier coatings, will be used to illustrate the concept of cycle jumps. However, the method developed can be applied to any system with evolving structural properties.

2.1. Example of a system with evolving material properties

In this section, we will describe some of the pertinent details of the materials systems considered: Thermal Barrier Coatings (TBCs), used in the hot part of gas turbine engines. Extensive reviews of these systems can be found for example in [20–23], and some of the key aspects of TBCs will be summarized in the following (as it pertains to this work).

TBCs enable higher operating temperatures, thus increased fuel efficiency. Through active internal cooling of the gas turbine blades and vanes, a thermal gradient is sustained over the TBC. The TBC consist of two layers (Fig. 2) deposited on the super alloy: (i) A metallic, aluminum rich, bond coat providing oxidation resistance; and (ii) a ceramic topcoat (typically yttria stabilized zirconia, YZT) providing thermal protection. Depending on the application, each layer is typically 75–200 μm thick. The bond coat oxidizes during exposure to the high operating temperatures, forming a thin oxide scale (predominantly alumina, Al_2O_3) in the interface between the bond coat and the top coat. The thermally grown oxide (TGO) is initially less than 0.5 μm and grows up to 7–10 μm before failure. As the TGO grows – depleting the bond coat on aluminum – the structure evolves: interfacial cracks initiate, grow and coalesce, leading to final spallation of the coating. Moreover, due to the aluminum depletion, the properties in the bond coat changes with time. Thus, fatigue failures of TBCs are typically associated with thermal cycling, inelasticity (e.g., creep and plasticity), and material evolution, finally leading to spallation of the coating.

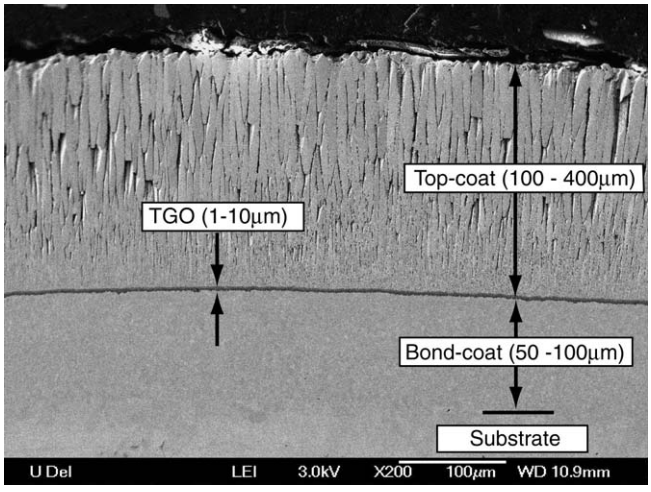

Fig. 2. A cross section of a thermal barrier coating before thermal exposures (courtesy Jin Yan, University of Delaware and Marion Bartsch, the German Aerospace Center).

One particular failure evolution in TBCs is related to morphological instability of the TGO, characterized by local imperfections in the TGO that grow on a cyclic basis, eventually causing crack propagation in, and spallation of, the top coat, e.g. [1,19,24–28]. The morphological instabilities develop during thermal cycling and not during isothermal conditions. Thus, the cyclic response is critical to simulate. This failure mechanism is driven by a combination of three non-linear constitutive behaviors in the coating: (1) high temperature inelasticity in the TGO, (2) growth strain in the TGO, and (3) cyclic yielding in the bond coat. The growth strain is induced due to the oxidation process when the new alumina is formed. The high temperature inelastic strength of the TGO is often referred to as "growth stress." The lateral component of the growth strain is limited by the growth stress and once the TGO stress reached the level of the growth stress, the lengthening strain is reallocated into thickening strain. The growth stress can be measured experimentally [29–31].

In this paper, we will use morphological instabilities as a sample problem since this failure mode is fairly well developed. However, the method we describe can be employed to any situation with evolving structure or properties.

2.2. Basic finite element model

In this feasibility study, we will investigate a two-dimensional finite element model, simulating a cylindrical geometry, Fig. 3A. The commercially available program ABAQUS [12] is used. The model is a variant of the model that was previously investigated by Karlsson and co-workers [10,19] to explore and explain morphological instabilities in TBCs. In this simplified model – designed to capture the necessary and sufficient parameters for morphological instabilities – only two of the coating's layers are present: the TGO in shape of a center ring, surrounded by the bond coat. To reduce the model size, only 1/4 of the circular cross section is meshed, and appropriate boundary conditions are applied, as indicated in Fig. 3A. In the current simulations, we assume generalized plane strain elements. When the morphological instabilities are considered, the radial change of the TGO-bond coat interface is monitored.

As described above, a key feature in the failure of TBCs is the formation and growth of the TGO. Thus, it is critical to model this behavior in a satisfactory manner, while maintaining a tractable numerical scheme. Here, we adapt a method developed previously [19,24,25]. In this model, the TGO is considered linear-elastic, ideal-plastic at growth, with yield strength σ_Y^{TGO} corresponding to the growth stress. Even though the real mechanism in the TGO is creep, the simplification serves to accumulate inelastic strain during each cycle [24,25]. The growth strain in the TGO, ε_g, is imposed as stress-free strain through the user subroutine UEXPAN [12]. The accumulation of growth strain is the component that drives this system. For simplicity, we will assume constant growth strain rate in each simulation.

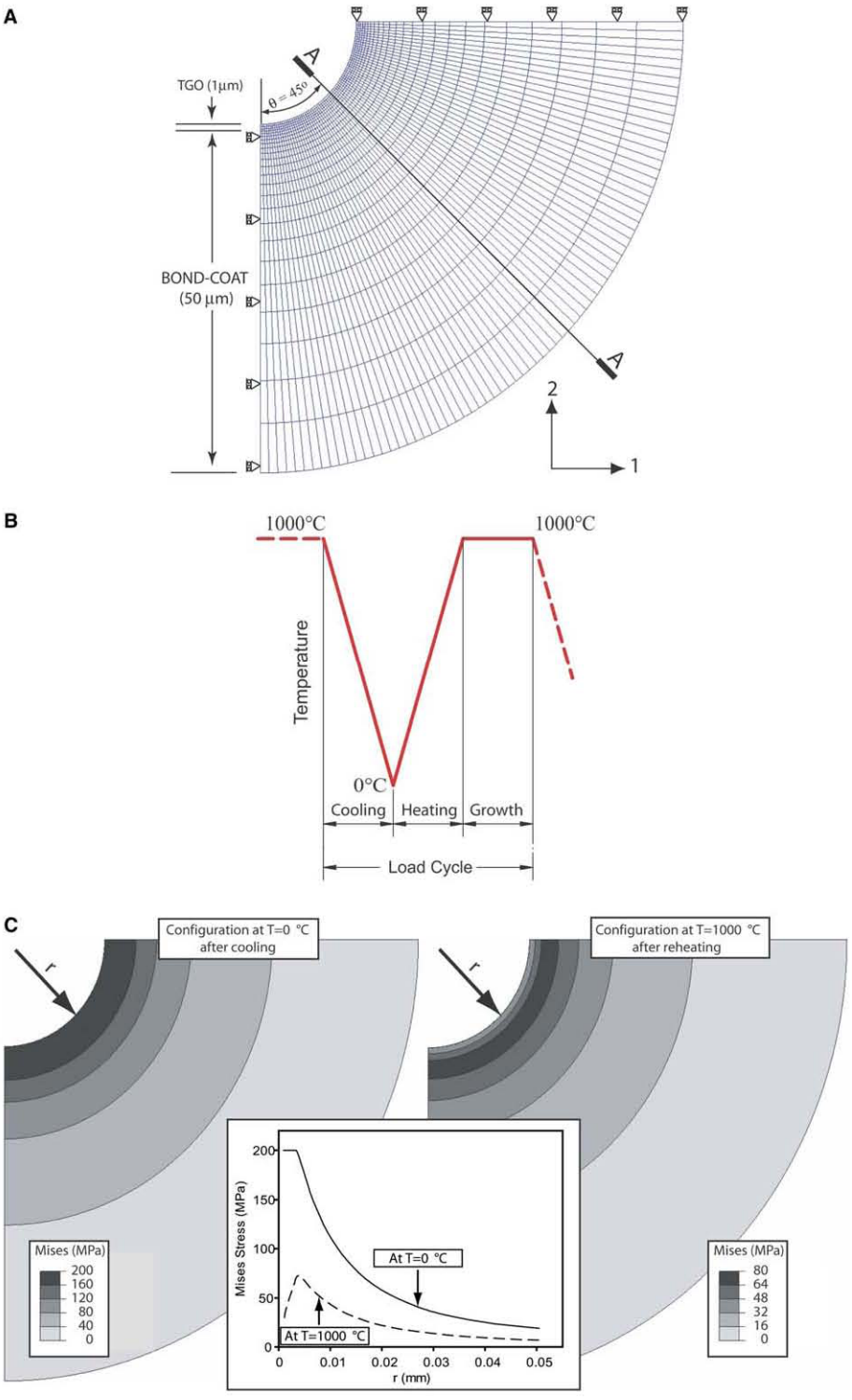

Fig. 3. (A) Finite element model used as a sample structure. State variables will be monitored along the line A–A. (B) Illustration of one load cycle. (C) Schematic of the general behavior of the Mises stresses in the bond coat during a cooling-heating cycle where $r = 0 \iff$ original inner TGO surface.

To maintain a tractable numerical scheme, we only assign evolving properties to the TGO in this feasibility study. However, as will be evident in the following, the method can incorporate any type of evolving material properties in multiple layers of the structure. Factors such as cyclic phase transformations [32] could also be incorporated.

Of particular interest is to explore the sensitivity for the heating-cooling sequence, which is approached in the following manner: The structure is initially stress-free at 1000 °C. Each thermal cycle consists of three parts: (1) cooling to 0 °C, (2) reheat to 1000 °C and (3) high temperature exposure at 1000 °C, where the TGO grows by

Table 1
Materials properties

Layer	Behavior	E (GPa)	ν	σ_Y (MPa)[a]	Thermal expansion $10^{-6} \times 1/°C$
Bond coat	Linear elastic–ideal plastic	190	0.3	200	14
TGO	Linear elastic–ideal plastic	380	0.2	10,000; $T \leqslant 900$ °C 1000; $T \geqslant 1000$ °C	8

[a] The yield strength for the TGO varies linearly in between the two temperature intervals. This property distribution allows the TGO to respond inelastic at elevated temperatures but elastic at all other temperature intervals.

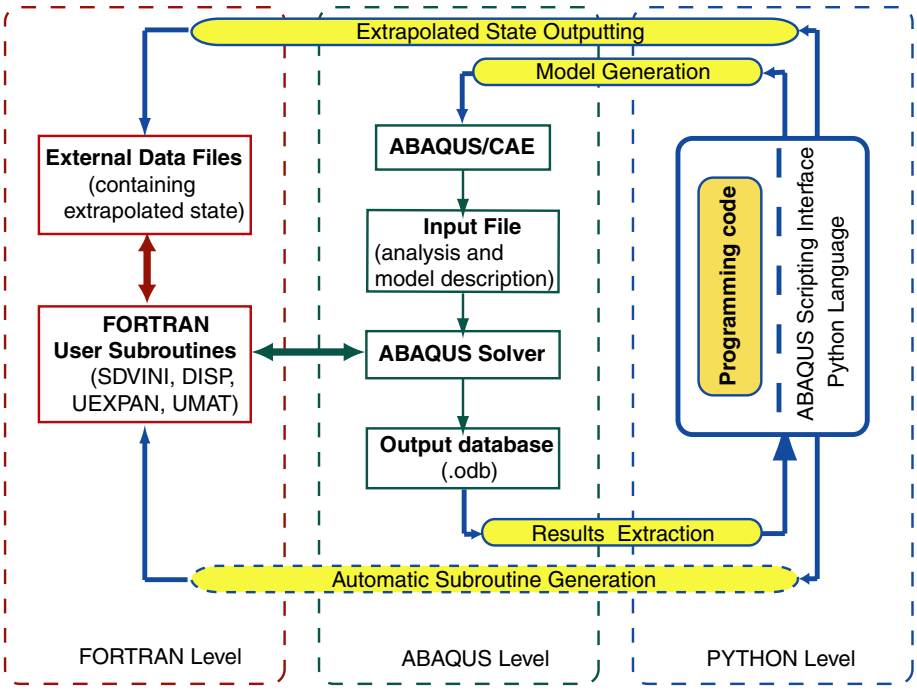

Fig. 4. A schematic of the implementation of cycle jumps.

imposing the stress-free strain. The loading sequence is illustrated in Fig. 3B. The material properties used are summarized in Table 1. We note that the system is driven by the sequence of cooling–heating–growth strain. Each cooling-heating cycle resets the system, allowing more growth strain to be imposed at high temperature [10,19]. A system subjected to isothermal conditions with the same accumulated time at temperature will not see a significant radial increase. The typical structural response is visualized in Fig. 3C, where the stresses according to von Mises is shown for the bond coat at 0 °C and 1000 °C. The yielding during cooling results in residual stresses after reheating. The TGO stresses are closed to 1 GPa (not shown for simplicity).

2.3. Implementation of cycle jumps to FEM-model

The basic FE-model is created using ABQUS/CAE and ABAQUS Scripting Interface (an extension to "Python" programming language)[12]. A schematic of the implementation and interaction between the various routines used is shown in Fig. 4. A set of cycles (including all necessary incremental steps) is conducted in ABAQUS. [1] Based on this solution, the "global evolution function" can be approximated. The "global evolution function" describes the extrapolation and the cycle jump is based on this function. All variables are extrapolated (stress, strain, displacement).

Since we cannot modify the information in the files containing the FEA results (e.g. the file "*.res"), the insertion of the extrapolated values into the FEA model by performing a "RESTART" command cannot be considered. Thus, we input the extrapolated values by utilizing the user-subroutine UMAT and prescribed displacements in user-subroutine DISP. The extrapolated displacements are applied at each node during the first step after extrapolation. These displacements are imposed incrementally (as if a displacement controlled loading was considered). During the last

[1] We note here that ABAQUS has a routine called "Direct Cyclic Analysis." This method predicts the steady state condition for transient problems, where the stresses eventually will cycle between constant values. The method presented in this paper, deals with a problem with evolving stress field, where stresses and strains (in general) will continue to change throughout the life.

increment in this step (at where the nodal displacements have reached the extrapolated displacements), the extrapolated stress and strain are imposed in the integration points. If a poor extrapolation was conducted, leading "too far away" from the equilibrium position, the analysis will fail to converge. This is the first indicator on how well the global evolution function extrapolated the cycles that were spanned. However, as will be seen later, convergence is not an indicator that a true solution is obtained. Indeed, an extrapolation scheme including a *control function* is needed to control the extrapolation function – both "slope" and "length." The formulation and behavior of the control function will be discussed next.

2.4. Extrapolation scheme

We present here a simple approach for an extrapolation scheme with a "control function," allowing the program to determine automatically a suitable length of the cycle jump. The method discussed here is most suitable for systems evolving in a quasi-linear manner. However, we will see that the extrapolation scheme will capture highly non-linear behavior of the evolving structure by automatically conducting shorter or no jumps. Thus, the extrapolation scheme compromises between the computational efficiency and the accuracy of the solution. The method described in the following will guide the program to automatically determine the length of the cycle jump, perform multiple jumps and – which will be seen in the result section – will stay close to the cycle-by-cycle solution. The control function developed here computes first the allowed jump-length for each variable in a control set at each integration point or/and node. The control set may contain all or a part of the variables involved in finite element analysis. The allowed jump length is computed based on an "accuracy control value," which has to be specified by the user for *each* variable used in the control set. The minimum of all the allowed jump length values is selected as the common jump length and is used to perform the jump. Details of the procedures are described in the following.

Let us consider the method for computing the jump length for *each* variable extrapolated. Assume that a FE-based solution has been obtained such that it contains at least two, up to N_c, computed loading cycles. For each variable, y, of interest (e.g. components of stress, strain, displacement), $y = y(t, \mathbf{M})$, where t is the time and $\mathbf{M}$ is any material point in the structure, at least three consecutive characteristic values are available. By characteristic values, we understand that those values are taken from the same relative position in time within the loading cycle.

For simplicity, we assume that the three values are extracted at the end of three consecutive cycles, and are defined by the points $P_1(t_1, y_1)$, $P_2(t_2, y_2)$, $P_3(t_3, y_3)$, Fig. 1.[2] From these values, information pertaining to the global evolution of variable y can be extracted. The increments by which the variable y changed during the last two cycles are $\Delta y(t_1) = y_1 - y_2$ and $\Delta y(t_2) = y_2 - y_3$, respectively. Alternatively, expressed in terms of discrete slopes, we have $s_{12}(t_1) = \Delta y(t_1)/\Delta t_{\text{cycle}}$ and $s_{23}(t_2) = \Delta y(t_2)/\Delta t_{\text{cycle}}$ respectively, where $\Delta t_{\text{cycle}} = t_1 - t_2 = t_2 - t_3$ represents the cycle length.[3]

The allowed jump length for each extrapolated parameter is dictated by the following criterion:

$$\frac{|s_p(t_1 + \Delta t^{\mathbf{M}}_{y,\text{jump}}) - s_{12}(t_1)|}{|s_{12}(t_1)|\leftarrow} \leqslant q_y, \tag{1}\leftarrow$$

where q_y is a relative error $(q_y > 0)$, $\Delta t^{\mathbf{M}}_{y,\text{jump}}$ is the time spanned by the jump for material particle $\mathbf{M}$, and $s_p(t_1 + \Delta t^{\mathbf{M}}_{y,\text{jump}})$ is the predicted slope at the moment after the jump, obtained by linear extrapolation as:

$$s_p(t_1 + \Delta t^{\mathbf{M}}_{y,\text{jump}}) = s_{12}(t_1) + \frac{s_{12}(t_1) - s_{23}(t_2)}{\Delta t_{\text{cycle}}}\leftarrow \Delta t^{\mathbf{M}}_{y,\text{jump}}. \tag{2}$$

Thus, the algorithm, by means of relation (1), ensures that the predicted slope at the time after the jump will be "close enough" to value of the slope before the attempted jump.

The value of q_y is a user specified input parameter and may be different for each variable in the control set. In our approach, we consider q_y as a constant, but it could also be a time dependent and automatically controlled parameter. The appropriate values of q_y can be obtained by comparing cycle-by-cycle analysis to a jump analysis for the initial portion of simulation (i.e. a reasonable number of cycles).

The value of allowed jump length is now easily obtained by substituting Eq. (2) into Eq. (1), and considering that the time-increments can have only positive values:

$$\Delta t^{\mathbf{M}}_{y,\text{jump}} = q_y \Delta t_{\text{cycle}} \frac{|s_{12}(t_1)|}{|s_{12}(t_1) - s_{23}(t_2)|}\leftarrow. \tag{3}$$

So far, we have considered the computation of the allowed jump length for each variable in the control set, at each material point (integration point). However, the cycle jump length computed at each point will not be the same for all parameters considered. Since q_y is supplied by the user, the most simple and efficient way to determine the common jump length, Δt_{jump}, is to set it as the minimum of the computed allowed jump length for each variable[4]

$$\Delta t_{\text{jump}} = \Delta t_{\text{cycle}} \lfloor \min\{\Delta t^{\mathbf{M}}_{y,\text{jump}}\}/\Delta t_{\text{cycle}} \rfloor, \tag{4}\leftarrow$$

[2] The minimum required number of consecutive cycles computed by finite element analysis is two, since P_3 (t_3, y_3) can be taken at beginning of the first FEA computed cycle.

[3] For simplicity, in examples presented in this work, the cycle length is considered constant although this is not a restriction for the method as long as the cycle length $\Delta t_{\text{cycle}}(t)$ is much smaller than the life time of the structure.

[4] We mention here that in [18] a statistical approach is used to calculate the global jump length once the local computation has been done. This might be seen redundant in the context of the criterion proposed in this paper.

where $\lfloor g \rfloor$ denotes the floor function (thus, returning the greatest integer less than or equal to g) and Δt_{jump} is the global jump length.

Finally, the algorithm uses the Heun integrator to perform the extrapolation of all the variables necessary for the next finite element analysis (after the cycle jump):

$$y(t_1 + \Delta t_{\text{jump}}) = y(t_1) + \frac{1}{2}[s_{12}(t_1) + s_{\text{p}}(t_1 + \Delta t_{\text{jump}})]\Delta t_{\text{jump}} \tag{5}$$

or, by substituting Eq. (2) (where now $\Delta t^{\mathbf{M}}_{y,\text{jump}}$ is replaced by Δt_{jump}) into (5), we get:

$$y(t_1 + \Delta t_{\text{jump}}) = y(t_1) + s_{12}(t_1)\Delta t_{\text{jump}} + [s_{12}(t_1) - s_{23}(t_2)]\frac{(\Delta t_{\text{jump}})^2}{2\Delta t_{\text{cycle}}}. \tag{6}$$

Higher order formulas can be used as well in order to perform the extrapolation, but they require more consecutive computed cycles by finite element analysis. In addition, the cycle length must be sufficiently small compared to the total time covered by the analysis, such that the approximation of the derivatives involved in describing the global evolution by using the per-cycle incremental information provided by finite element analysis to remain accurate.

The number of intermediate full cycles simulated by FEA (after one jump, before the next), $N_{\text{FEA},j}$, is adjusted automatically based on the previously computed jump length. This adjustment is empirical and can be expressed as

$$\begin{aligned} &N_{\text{FEA},j} = N_{\text{FEA},j-1} + \Delta_+, \text{ if } (\Delta t_{\text{jump},j}/\Delta t_{\text{cycle}}) \leqslant 1, \\ &N_{\text{FEA},j} = N_{\text{FEA},j-1} - \Delta_-, \\ &\quad \text{if } (\Delta t_{\text{jump},j}/\Delta t_{\text{cycle}}) \geqslant N_{\text{FEA},j-1} \text{ and } N_{\text{FEA},j-1} - \Delta_- \geqslant N_{\min}, \\ &N_{\text{FEA},j} = N_{\text{FEA},j-1}, \quad \text{otherwise.} \end{aligned} \tag{7}$$

where j is jump that was just performed. Δ_+ and Δ_- are user supplied parameters, representing the increase and decrease, respectively, in the number of FE computed cycles, and $N_{\min}$ represents the minimum allowed $N_{\text{FEA},j}$ ($j = 1, 2, \ldots$). This approach aims to minimize unnecessary jump computation when the global evolution is highly non-linear.

Having established the controlled cycle-jump procedure, it is now of interest to investigate how various factors might influence the extrapolation accuracy and the computational efficiency. These issues together with the importance of having a reasonable procedure for determining the jump length are addressed and presented in the following section.

3. Results

3.1. Reference simulation

Two reference simulations were conducted which include all individual cycle increments and steps required to reach the targeted time (or number of cycles). The reference calculations are used for comparison of the cycle jump simulations, to access the accuracy of the technique. None of the results from the reference simulations were used when conducting the cycle jump simulations.

In both simulations, 500 cycles (i.e., 1500 Abaqus steps: one load cycle constituting three Abaqus steps, Fig. 3B) were calculated. The two cases considered are "low growth strain rate," $\varepsilon_{\text{g}} = 10^{-4}$ and "high growth strain rate," $\varepsilon_{\text{g}} = 10^{-3}$, where the growth strain rate corresponds to the amount of growth strain applied during each cycle. The lengthening and thickening component of the growth strain are assumed to equality, for simplicity. The eigenstrain imposed in the TGO drives the system, making the state parameters evolve with each cycle.

Consider the evolution of stresses and plastic strain in a material element (integration point) on the bond coat, close to the TGO, Fig. 5. For both low and high growth strain rate, the effective stress according to von Mises, "Mises stress," starts at zero stress, reaches a maximum when the low temperature is reached (0 °C), decreases as the structure is reheated (back to 1000 °C), and increases when the growth strain is applied during the first cycle (Fig. 5A). This is the local response for the structure, repeated for each cycle. However, the values of the maximum and minimum stresses change as the structure is cycled. This behavior corresponds to the global evolution of the structure. In particular, we see that the Mises stress increases on a cyclic basis until yield is reached after about seven cycles for the case of low growth strain rate (Fig. 5A). When high growth strain rate is considered, the material element reaches yield

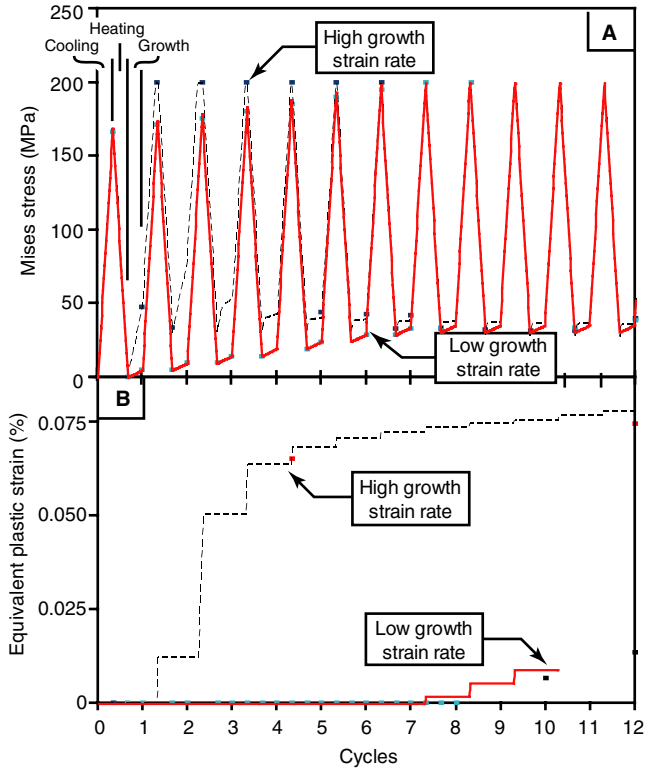

Fig. 5. Evolution over the first 12 cycles of (A) Mises stress and (B) equivalent plastic strain, in a bond coat element next to the TGO interface.

during the second cycle. For both cases, the stress at the lower temperature is constant after yielding has occurred, at 200 MPa corresponding to the yield strength of the material, whereas the stresses at the higher temperature continue to change slightly with each cycle.

The non-linear constitutive response can easiest be monitored by considering the plastic strain. To this end, we will monitor the *equivalent plastic strain* ε^{p}_{eq}, for classic plasticity theory defined as [33]

$$\varepsilon^{p}_{eq} = \int \left(d\varepsilon^{p}_{eq} \equiv \int \left(\left[\frac{2}{3} d\varepsilon^{p}_{ij} d\varepsilon^{p}_{ij} \right] \right)^{1/2} \right) \tag{8}$$

where $d\varepsilon^{p}_{eq}$ is the equivalent plastic strain increment and $d\varepsilon^{p}_{ij}$ are the individual components. (The equivalent plastic strain should not be confused with *current plastic strain* which takes the sign of deformation into consideration [19]). For the case considered, the equivalent plastic strain accumulates with each cycle after yielding has occurred (Fig. 5B). Significant more equivalent plastic strain accumulates for the high growth strain rate.

The long term behavior is illustrated in Figs. 6–8, where the states after the high-temperature growth strain application steps are shown. Again, let us consider the evolution of the Mises stress and the equivalent plastic strain, but this time we will view it as a function of the radius along the 45° line (as indicated in Fig. 3). For low growth strain rate, Fig. 6A, a stress maximum is seen close to $r = 10$ μm. The location of maximum stress corresponds to the location of the plastic zone during the cooling step. The yield zone moves toward higher radii with each cycle (Fig. 6A and B). Thus, most of the structure remains elastic during the 500 cycles. The scenario for the high growth strain rate changes somewhat (Fig. 7A and B). In this case, the plastic zone moves rapidly towards the edge of bond coat as the structure is cycled, resulting in overall yielding after 283 cycles. After this time, overall yielding will occur at each cycle (at low temperature).[5]

The development of the plastic zone directly influences the radial displacement of the boundaries, elucidated in Fig. 8. In this Figure, the evolution of the inner TGO surface and the TGO/BC interface are monitored as a function of time. For the case of low growth strain rate, the location

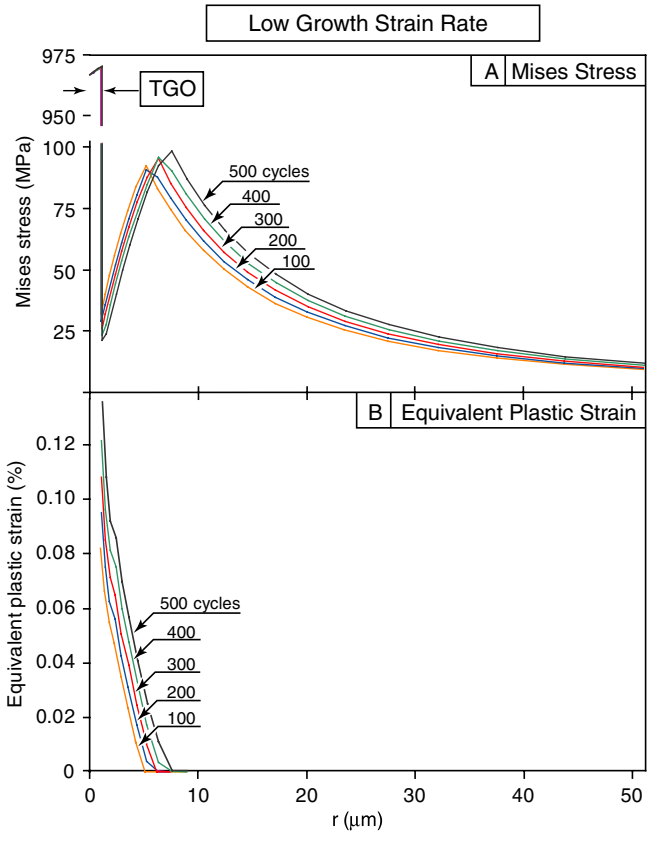

Fig. 6. For low growth strain rate, example of results from reference simulation: (A) evolution of Mises stresses and (B) evolution of equivalent plastic strain; up to 500 cycles. State shown after high temperature exposure (1000 °C), along the line A–A in Fig. 3. $r = 0 \iff$ original inner TGO surface.

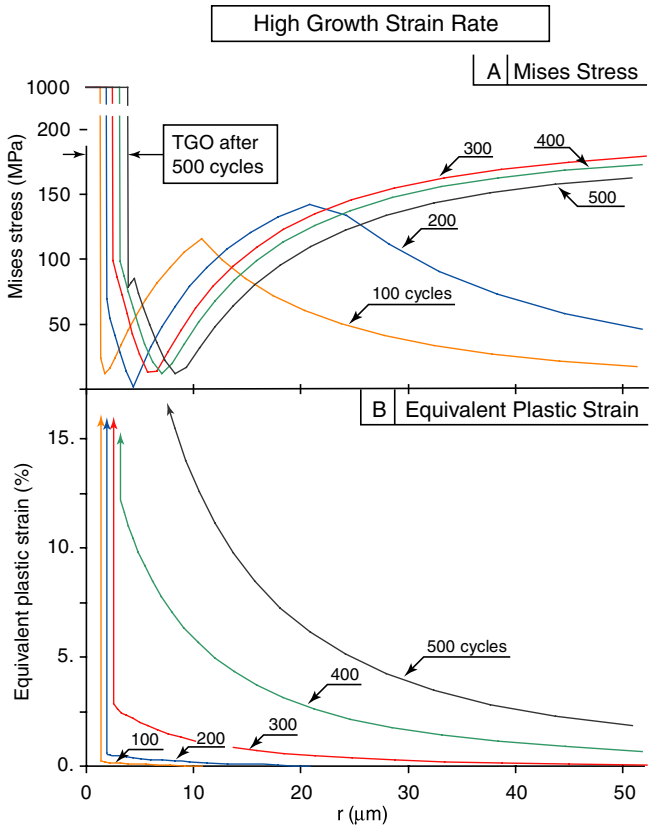

Fig. 7. For high growth strain rate, example of results from reference simulation: (A) evolution of Mises stresses and (B) evolution of equivalent plastic strain; up to 500 cycles. State shown after high temperature exposure (1000 °C), along the line A–A in Fig. 3. $r = 0 \iff$ original inner TGO surface.

[5] We note that this model does not give a true behavior of the TBC system. Overall yielding in the bond coat is frequently observed, e.g. [27,28]. However, this is associated with a driving force from the constraint the substrate imposes or due to a thermal gradient, which is not included in the current model. In the present case, overall yielding occurs due to small size of the bond coat modeled.

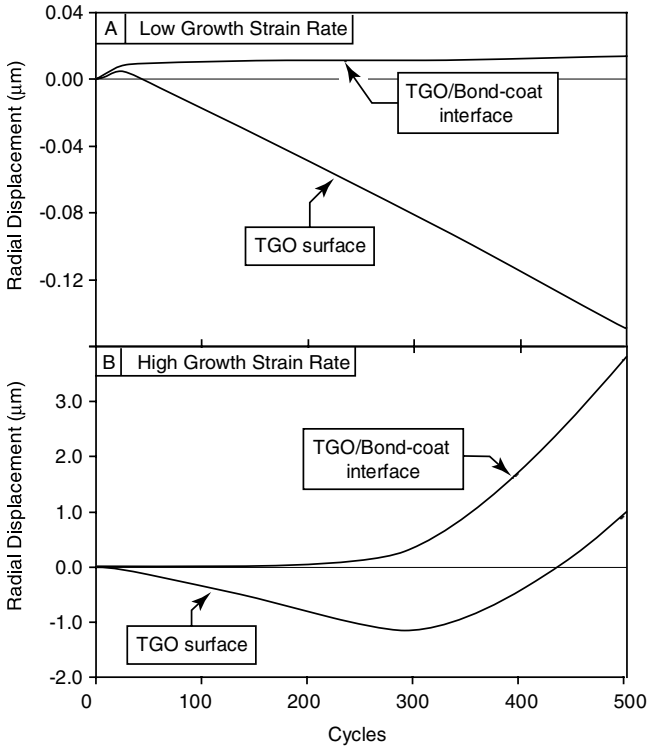

Fig. 8. Radial displacement as a function of time for (A) low growth strain rate and (B) high growth strain rate.

of the TGO/bond coat moves slightly outwards, whereas the inner surface moves towards the center of the cylinder. The case of high growth strain rate initially replicates the behavior of low growth strain rate. However, as the structure is cycled, both surfaces displace significantly, including a direction reversal of the inner surface. The direction reversal is associated with the onset of overall yielding and this non-linear behavior may cause a challenge for the cycle jump simulations. In both cases, the thickness of the TGO increases, manifested as the difference between the two lines shown in the Figure. After 500 cycles, the TGO has increased in thickness with 0.163 μm and 2.842 μm (hence, the final TGO-thickness of 1.163 μm and 3.842 μm) for low and high growth strain rate, respectively.

3.2. Accuracy of results without control

We will now investigate cycle jumps conducted without a control function and compare the results to the reference simulations. This will show that even if the finite element analysis converges after the cycle jump, it does not necessarily mean that an acceptable solution is achieved (that is, a solution that is close to the true solution).

To this end, we will study the case of the higher growth strain rate and conduct an uncontrolled jump. The global extrapolation function in this case is based on 20 initial "complete cycles." ("Complete cycles" refers to that all increment and all three steps are computed through regular FEA.) The extrapolation is performed using relation (5), with the jump length set to $\Delta t_{\text{jump}} = 274$ cycles. After the 274 long cycle jump, six additional full cycles are conducted. (We will later see that complete cycles after a cycle jump tend to bring the solutions closer to the true solution.) Thus, 300 cycles are simulated with one cycle jump, and 20 initial and 6 final FEA calculated cycles. Comparing the results from the cycle jump to the reference calculation, Fig. 9, it is evident that the Mises stress is not correct for larger coordinates ($r > 32$ μm), and that the plastic strain in the bond coat is off by a factor of about three for all locations. Obviously, the cycle jump does not capture the larger region of yielding that has evolved in the bond coat. Thus, convergence after a cycle jump does not guarantee a true solution.

3.3. Cycle jumps with control

Next, we will discuss the results achieved when implementing the extrapolation scheme containing control function as described in Section 2. In all cases, 500 cycles are simulated and compared with the reference simulations. Tables 2 and 3 summarizes the simulations conducted for low and high growth strain rate, respectively. Here, the control set includes only the displacements components, u_1 and u_2, i.e., deformation in the (global) x- and y-direction, respectively. However, the set could contain any state variable, such as stress and/or strain tensors components.

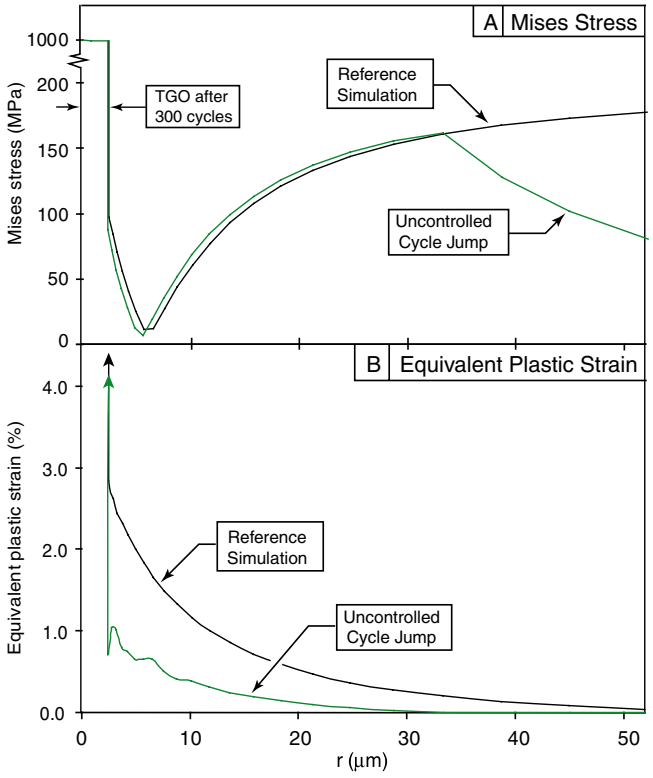

Fig. 9. For high growth strain rate, an uncontrolled jump compared to the reference simulations: (A) Mises stress and (B) equivalent plastic strain; 300 cycles, one jump spanning 274 cycles. State shown after high temperature exposure (1000 °C), along the line A–A in Fig. 3. $r = 0 \iff$ original inner TGO surface.

Table 2
For low growth strain rate, computational efficiency of various control parameters and requirement of minimum number of cycles after cycle jump

Control parameters $q_{u_1} = q_{u_2}$	Min. FEA length $N_{\min}$ (cycles)	Average of MISES relative error (%)	Standard deviation of MISES relative error	Average of EQPL relative error (%)	Standard deviation of EQPL relative error	Jump computed life L_{jumps} (cycles)	Number of jumps occurred	R
–	500	–	–	–	–	0	0	0
0.1	6	0.010889	0.015444	0.019135	0.044932	327	16	0.654
0.05	6	0.008663	0.010715	0.015371	0.036293	308	16	0.616
0.25	6	0.02559	0.028599	0.065686	0.117517	360	16	0.72
0.5	6	0.064814	0.0759	0.170201	0.414964	365	17	0.73
2.0	6	2.484124	12.23857	9.962509	75.90268	358	17	0.716
0.1	2	0.04128	0.034898	0.02924	0.094727	339	19	0.678
0.1	4	0.041064	0.036803	0.028876	0.1893	344	20	0.688
0.1	8	0.009359	0.013736	0.017445	0.038351	309	14	0.618
0.1	10	0.011699	0.011691	0.021022	0.050742	320	13	0.64
1.0	6	0.359965	2.261973	3.25676	16.38999	347	19	0.694

Table 3
For high growth strain rate, computational efficiency of various control parameters and requirement of minimum number of cycles after cycle jump

Control parameters $q_{u_1} = q_{u_2}$	Minimum FEA length $N_{\min}$ (cycles)	Average of MISES relative error (%)	Standard deviation of MISES relative error	Average of EQPL relative error (%)	Standard deviation of EQPL relative error	Jump computed life L_{jumps} (cycles)	Number of jumps occurred	R
–	500	–	–	–	–	0	0	0
0.1	6	0.056103	0.052195	0.17492	0.085305	164	24	0.328
0.25	6	0.154843	0.136927	0.441524	0.308594	313	19	0.626
0.5	6	0.477505	0.729945	0.386546	0.490643	338	20	0.676
1	6	1.691285	2.853201	0.908853	0.661796	380	13	0.760
2.0	6	3.57598	3.739328	3.691796	2.266767	412	9	0.824
0.5	2	0.379698	0.379698	0.408386	0.534336	322	28	0.644
0.5	10	0.185574	0.242929	0.728369	0.419562	356	12	0.712
0.1	2	0.075744	0.07138	0.21694	0.08928	189	29	0.378
0.25	2	0.12242	0.108115	0.275301	0.174854	263	30	0.526

In the following, for each growth strain rate, the control parameters q_{u_1} and q_{u_2} are varied to investigate the sensitivity for these parameters on the solution. The influence of minimum number of intermediate full cycles, $N_{\min}$, is also investigated. To this end, the following values (for Eq. (7)) in cycles, have been used throughout: $\Delta_+ = 2$, $\Delta_- = 1$.

The evolution of the structure during the simulation when subjected to high growth strain rate is illustrated in Fig. 10, where the radial component of the interface between the TGO and the bond coat is monitored as a function of time (cycles). The results from the simulations using the cycle jump technique are compared to the reference configuration in this graph. Fig. 10 shows that the surface moves inwards (negative displacements) during the first part of the simulations, but will move outwards (positive displacements) after about 300 cycles, a behavior observed earlier in Fig. 8. The transition induces a strong non-linear response. The cycle jump technique captures this behavior well by conducting shorter cycle jumps or no jumps during the mostly non-linear part of the sequence and automatically making longer jumps during the mostly linear sequence.

In addition to monitoring the displacement, as in Fig. 10, we can study state variables such as stress and strain. For example, from the Mises stress and equivalent plastic strain along the 45° line of the structure (Figs. 11 and 12), it is evident that these state parameters are "close" to the reference simulations. In fact, all solutions listed in Tables 2 and 3 overlap the reference simulations except the case of $q_{u_1} = q_{u_2} = 2.0$, thus we only display two cases in Figs. 11 and 12. For $q_{u_1} = q_{u_2} = 2.0$ the solution obtained from the jump simulation deviates from the reference simulation.

To quantify the computational efficiency from the cycle jump technique, we introduce the ratio:

$$R = L_{\text{jumps}}/L_{\text{tot}}, \tag{9}$$

where L_{jumps} is the total time covered by the jumps and L_{tot} is the total time considered for the analysis. Thus, the more efficient (e.g., longer jumps) a calculation is, the higher value of R. Generally, the computational efficiency increases with increasing value of the control parameters (Tables 2 and 3). However, the accuracy of the calculation based on cycle jumps compared to the reference calculation, decreases with increasing value of the control parameters.

The accuracy, or errors, of the cycle jump simulations can be determined by comparing the results to the reference simulations. The errors can be quantified by considering the relative error of the state variables. The relative error, δE, is defined by

$$\delta E = \left| \frac{y_{\text{ref}} - y_{\text{jump}}}{y_{\text{ref}}} \right| \times 100\ (\%), \tag{10}$$

where y is the value of the state parameter at the integration point, and indexes ref and jump indicate reference

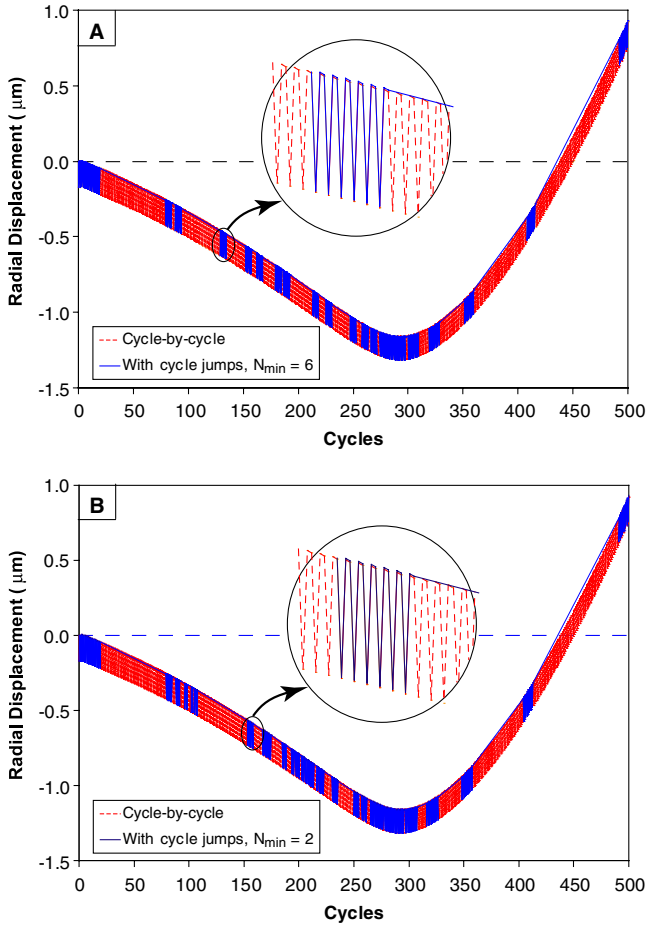

Fig. 10. Displacement of inner TGO surface as a function of cycles for high growth strain rate, reference case compared to the cycle jump technique, after (equivalent of) 500 cycles. Requirement of minimum cycle jumps as (A) 6 and (B) 2. $q_{u_1} = q_{u_2} = 0.5$, high growth strain rate.

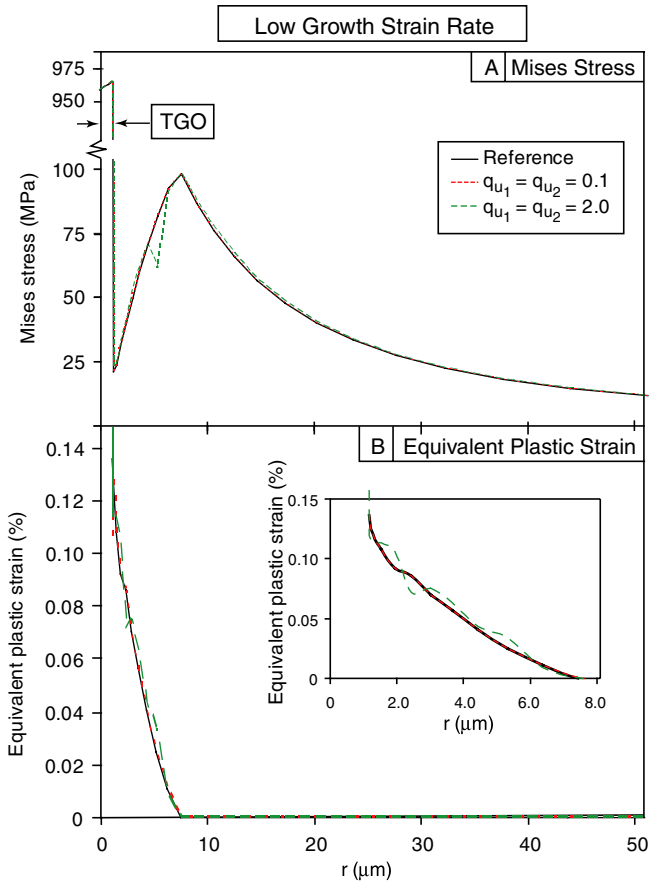

Fig. 11. For low growth strain rate, the cycle jump technique ($q_{u_1} = q_{u_2} = 0.1$ and 2.0) compared to the reference simulation after (equivalent of) 500 cycles: (A) Mises stress and (B) equivalent plastic strain (insert show an enlargement of the region $0 \leqslant r \leqslant 8$ μm). State shown after high temperature exposure (1000 °C), along the line A–A in Fig. 3. $r = 0 \iff$ original inner TGO surface.

and cycle-jump based simulation, respectively. One way to represent the overall error of the jump model is to consider the average relative error,

$$\overline{\delta E} = \frac{\sum_N \delta E}{N} \tag{11}$$

and the standard deviation of the relative error

$$s = \sqrt{\frac{\sum_N (\delta E - \overline{\delta E})^2}{N}}, \tag{12}$$

where $N = 16207$ is the total number of integration points in the model. From Tables 2 and 3, we see that both the average and the standard deviation of the relative error increase for both Mises stresses and equivalent plastic strain, for both growth strain rates, as the control parameters increase.

A careful evaluation of Fig. 10 shows that the intermediate, complete cycles between the jumps tend to bring the solution back towards the results from the reference simulations. This suggests that conducting more intermediate simulations will in general increase the accuracy of the simulation. In this case, the accuracy does not compromise the computational efficiency, as seen in Tables 2 and 3.

At present, we have not verified the numerically achieved results experimentally. We assume that the solution obtained by the cycle-by-cycle finite element simulations is correct (within the context of the physical problem defined). Thus, when the cycle-jump scheme gives the same solution as the cycle-by-cycle solution, the cycle-jump technique developed here is considered correct.

3.4. Cycle jumps beyond the reference simulations

Last, we present results from a simulation beyond the reference simulation. For the case of low growth strain rate, a simulation corresponding to 7000 cycles was conducted.

In this case the control parameter values were set to $q_{u_1} = q_{u_2} = 0.25$ for the first 2000 cycles, then to $q_{u_1} = q_{u_2} = 0.15$ for the analysis segment between 2000 and 3500 cycles and to $q_{u_1} = q_{u_2} = 0.05$ for the final portion, between 3500 and 7000 cycles. By studying the equivalent plastic strain (Fig. 13B), it is seen that the structure

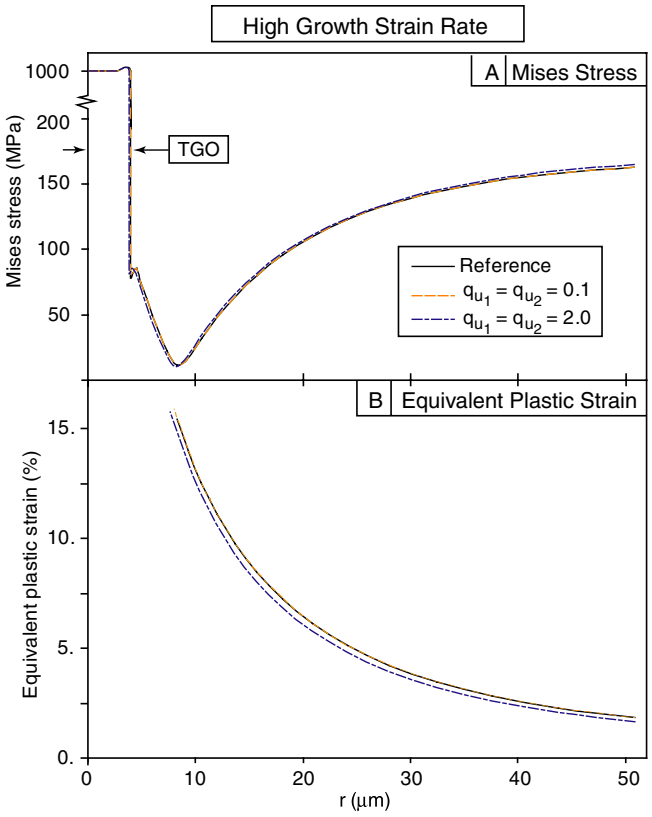

Fig. 12. For high growth strain rate for a controlled jump ($q_{u_1} = q_{u_2} = 0.1$ and 2.0) compared to the reference simulations for (equivalent of) 500 cycles. (A) Mises stress and (B) equivalent plastic strain. State shown after high temperature exposure (1000 °C), along the line A–A in Fig. 3. $r = 0 \iff$ original inner TGO surface.

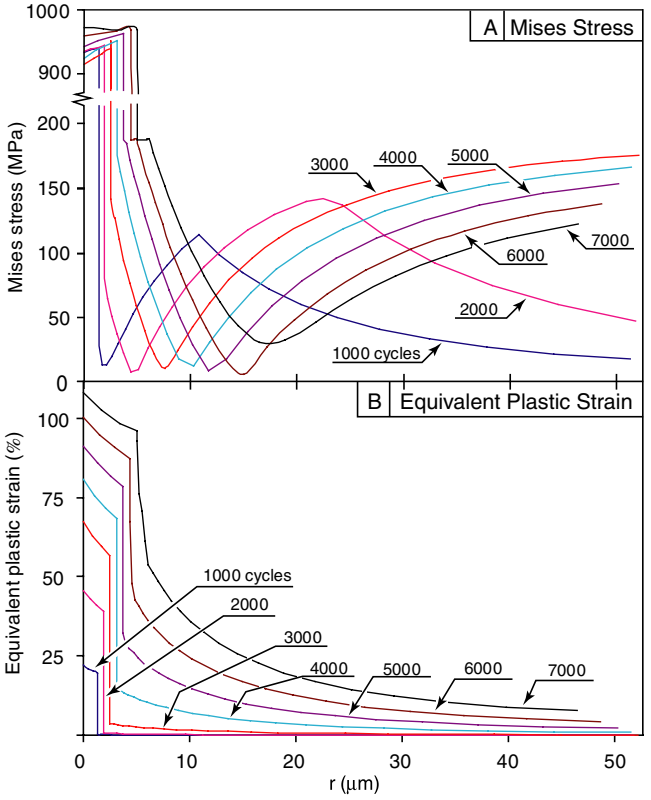

Fig. 13. For low growth strain rate, simulation of up to 7000 cycles: (A) evolution of Mises stresses and (B) evolution of equivalent plastic strain. State shown after high temperature exposure (1000 °C), along the line A–A in Fig. 3. $r = 0 \iff$ original inner TGO surface.

slowly moves from elastic–plastic state, to experience overall yielding after about 3000 cycles. The evolution of the Mises stresses (Fig. 13A) concur with this, showing similar response as when the higher growth strain rate was used in which case overall yielding was observed. In this case, we cannot access the accuracy of the results, since no reference simulation exists.

The modification of control parameters was required since in a long analysis the selected values of the control parameters became too large, leading to inaccurate extrapolation at the end of very long cycle jumps. This situation is easy correctable in our extrapolation scheme. We selected to reduce the values of the control-parameters and restarting the analysis from a moment when the solution still was considered accurate. Alternatively, a maximum allowed jump length could be imposed. Both methods may be performed automatically by the code, analyzing the FEA response immediately after a jump. By studying the finite element solution in the first cycle after a jump, the jump accuracy validation can be performed and the jump computation procedure can be restarted with modified control parameters, this procedure being the subject of our in-progress work. We are currently extending the code to incorporate an automatic adjustment of the control parameters.

4. Concluding remarks

A method for accelerated numerical simulations of structures subjected to cyclic loading has been developed and is presented in this paper. Of particular interest is a class of structures where the properties evolve with time. As inspiration for the work, we have used a common failure evolution seen in thermal barrier coatings, referred to as morphological instabilities or "ratcheting," even though the proposed method is applicable to a range of systems where the structural properties evolve, including incorporating damage parameters.

The method discussed and developed in this work is based on combining a cycle jump technique with finite element simulations. A key part of the technique is an extrapolation scheme, containing a control function, allowing the program to automatically determine a suitable length of the cycle jump, performing multiple jumps and ensuring that the solution is accurate. By user-input, the control function can be controlled through a parameter that defines an allowable error. Thus, the extrapolations scheme compromises between computational efficiency and accuracy of the solution. To visualize the accuracy of the proposed method, a reference simulation is conducted, containing all increments and steps. However, knowledge from this simulation is only used to verify the results.

The method discussed here is most suitable for systems evolving in a quasi-linear manner. However, it is seen that the extrapolation scheme will capture highly non-linear behavior of the evolving structure by automatically conducting shorter or no jumps. Thus, the method stays close to the solution obtained from the cycle-by-cycle simulation even with high non-linear evolution, however compromising the computational efficiency.

In all, we show that this relatively simple approach to accelerated numerical simulations, capturing the development and evolution of structures subjected to cyclic loading, can give reliable solutions while saving significant computational efforts.

Acknowledgement

The authors would like to acknowledge that this work was supported by ONR-N00014-04-1-0498.

References

[1] Mumm DR, Evans AG, Spitsberg IT. Characterization of a cyclic displacement instability for a thermally grown oxide in a thermal barrier system. Acta Mater. 2001;49:2329–40.
[2] Rabiei A, Evans AG. Failure mechanisms associated with the thermally grown oxide in plasma-sprayed thermal barrier coatings. Acta Mater 2000;48:3963–76.
[3] Wang R, Mercer C, Evans AG, Cooper CV, Yoon HK. Delamination and spalling of diamond-like-carbon tribological surfaces. Diamond and Related Materials 2002;11:1797–803.
[4] Tang Y, Santare MH, Karlsson AM, Cleghorn S, Johnson WB. Stresses in proton exchange membranes due to hydration-dehydration cycles. Journal of Fuel cell Science and Technology, in press.
[5] Gougeon N, Poulain M, El Abdi R. Evolution of strength silica optical fibers under various moisture conditions. Opt Mater 2004;27:75–9.
[6] Evans AG, Hutchinson JW. The thermomechanical integrity of thin-films and multilayers. Acta Mater 1995;43:2507–30.
[7] Nguyen T, Martin J, Byrd E, Embree N. Relating laboratory and outdoor exposure of coatings: II. Effects of relative humidity on photodegradation and the apparent quantum yield of acrylic-melamine coatings. J Coat Technol 2002;74:65–80.
[8] Lee WY, More KL, Stinton DP, Bae YW. Characterization of Si3N4 coated with chemically-vapor-deposited mullite after Na2SO4-induced corrosion. J Am Ceram Soc 1996;79:2489–92.
[9] Lucas GE. The evolution of mechanical property change in irradiated austenitic stainless-steels. J Nucl Mater 1993;206:287–305.
[10] Karlsson AM, Hutchinson JW, Evans AG. The displacement of the thermally grown oxide in thermal barrier systems upon temperature cycling. Mater Sci Eng A 2003;351:244–57.
[11] Suresh S. Fatigue of materials. Cambridge University Press; 1998. p..
[12] ABAQUS, ABAQUS 6.5, ABAQUS Inc., Pawtucket, Rhode Island, 2004.
[13] Boisse P, Bussy P, Ladeveze P. A new approach in nonlinear mechanics – the large time increment method. Int J Numer Meth Eng 1990;29:647–63.
[14] Cognard JY, Ladeveze P, Talbot P. A large time increment approach for thermo-mechanical problems. Adv Eng Software 1999;30:583–93.
[15] Fish J, Yu Q. Computational mechanics of fatigue and life predictions for composite materials and structures. Comput Meth Appl Mech Eng 2002;191:4827–49.
[16] Oskay C, Fish J. Fatigue life prediction using 2-scale temporal asymptotic homogenization. Int J Numer Meth Eng 2004;61:329–59.
[17] Kiewel H, Aktaa J, Munz D. Application of an extrapolation method in thermocyclic failure analysis. Comput Meth Appl Mech Eng 2000;182:55–71.
[18] Van Paepegem W, Degrieck J, De Baets P. Finite element approach for modelling fatigue damage in fibre-reinforced composite materials. Composites Part B – Eng 2001;32:575–88.
[19] Karlsson AM, Hutchinson JW, Evans AG. A fundamental model of cyclic instabilities in thermal barrier systems. J Mech Phys Solids 2002;50:1565–89.
[20] Miller RA. Oxidation-Based Model for Thermal Barrier Coating Life. J Am Ceram Soc 1984;67:517–21.
[21] Strangman TE. Thermal Barrier Coatings for Turbine Airfoils. Thin Solid Films 1985;127:93–105.
[22] Evans AG, Mumm DR, Hutchinson JW, Meier GH, Petit FS. Mechanisms controlling the durability of thermal barrier coatings. Progr Mater Sci 2001;46:505–53.
[23] Padture NP, Gell M, Jordan EH. Materials science – thermal barrier coatings for gas-turbine engine applications. Science 2002;296:280–4.
[24] Karlsson AM, Evans AG. A numerical model for the cyclic instability of thermally grown oxides in thermal barrier systems. Acta Mater 2001;49:1793–804.
[25] Karlsson AM, Levi CG, Evans AG. A model study of displacement instabilities during cyclic oxidation. Acta Mater 2002;50:1263–73.
[26] Karlsson AM, Xu T, Evans AG. The effect of the thermal barrier coating on the displacement instability in thermal barrier systems. Acta Mater 2002;50:1211–8.
[27] Shi J, Darzens S, Karlsson AM. Aspects of the morphological evolution in thermal barrier coatings and the intrinsic thermal mismatch therein. Mater Sci Eng A 2005;392:301–12.
[28] Shi J, Karlsson AM, Baufeld B, Bartsch M. On the thermal cycling and evolution of surface morphology for thermally cycled NiCoCrAlY bond coats. 29th Int Conf Adv Ceram Composite 2005;26:65–72.
[29] Tolpygo VK, Dryden JR, Clarke DR. Determination of the growth stress and strain in alpha-Al2O3 scales during the oxidation of Fe–22Cr–4.8Al–0.3Y alloy. Acta Mater 1998;46:927–37.
[30] Schlichting KW, Vaidyanathan K, Sohn YH, Jordan EH, Gell M, Padture NP. Application of Cr(3+)photoluminescence piezo-spectroscopy to plasma-sprayed thermal barrier coatings for residual stress measurement. Mater Sci Eng A 2000;291:68–77.
[31] Tomimatsu T, Zhu SJ, Kagawa Y. Local stress distribution in thermally-grown-oxide layer by near-field optical microscopy. Scripta Mater 2004;50:137–41.
[32] Karlsson AM. On the mechanical response in a thermal barrier system due to martensitic phase transformation in the bond coat. J Eng Mater Technol – Trans ASME 2003;125:346–52.
[33] Hill R. The mathematical theory of plasticity. Oxford: Oxford University Press; 1950.